

Design, Fabrication, and Testing of Silicon Photonic MZI-Based Polymer Electro-Optic Modulators

Timothy Nguyen

Department of Electrical and Computer Engineering
University of British Columbia, Vancouver, BC V6T 1Z4, Canada

Abstract—Polymer electro-optic (EO) modulators were designed, fabricated, and tested to extract key figures of merit, namely the half-wave voltage V_π that is required to shift the response at the operating wavelength from maximum to minimum transmission. The devices were designed to minimize V_π in layout by employing a push-pull configuration and minimizing the separation between the metal electrodes used for poling and modulation. Unique fabrication steps included patterning using electron-beam lithography, physical vapour deposition of the metal layer using a custom-built electron-beam evaporator, and poling of the EO material. A successfully-fabricated modulator with modulation length $L = 3$ mm exhibited $V_\pi = 6.569$ V and $V_\pi L = 19.707$ Vmm.

I. INTRODUCTION

Modulators are a key component of integrated photonic communication systems involved in applications including biosensing, imaging, LIDAR, inertial sensing, hybrid photonic-RFICs, and signal processing [2]. Modulator performance depends on the device topology, materials used, and the underlying mechanism generating the phase shift. They are ranked on several figures of merit listed below:

- Modulation efficiency ($V_\pi L$)
- Insertion Loss
- Electro-optical -3 dB Bandwidth
- Power Consumption
- Footprint
- Fabrication Complexity

Silicon modulators currently produced in CMOS Si-on-insulator (SOI) foundries generate phase shift based on the free-carrier plasma dispersion (FCD) effect controlled by carrier depletion in PN junctions [3]. The electro-optic bandwidth of these FCD-modulated devices is limited to 50 GHz for a reasonable insertion loss [4]. In addition, they produce undesired intensity modulation and respond nonlinearly to the applied voltage.

Silicon-organic hybrid (SOH) modulators are a promising alternative to existing FCD modulators leveraging Pockel's effect. They consist of silicon waveguides clad in an organic electro-optic (EO) polymer. The main advantages of SOH modulators include half-wave voltages (V_π) as low as 0.25 V [6] resulting in lower power consumption and high bandwidth-length product ($f \times l$) of 150 GHz cm [7].

One disadvantage of SOH modulators is that it requires additional post-processing steps in the foundry. Devices after patterning are coated in polymer and then poled: the process aligning of chromophore molecules by an external electrical field at elevated temperatures. The additional manufacturing variability can lead to sub-optimal or non-functioning devices.

Investigation into the manufacturing variability in SOH modulator fabrication is crucial if the technology is to be introduced at CMOS foundries with high yield. Hence, students partaking in a Micro/Nanofabrication and Instrumentation Laboratory course at the University of British Columbia were asked to design and fabricate variations of polymer electro-optic Mach-Zehnder modulators, and then acquire experimental data to compare against simulated models. The project results are presented in subsequent sections.

II. THEORY & MODELLING

A. Mach-Zehnder Interferometer Theory

A non-slotted Mach-Zehnder modulator (MZM) topology was employed for phase modulation due to its simplicity in manufacturing. A passive Mach-Zehnder interferometer drawn in KLayout is shown in Fig. 1.

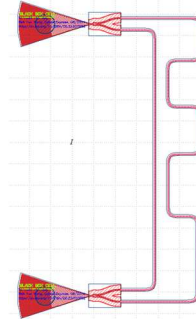


Figure 1. Passive Mach-Zehnder interferometer with equal propagation constants and unequal path lengths.

In essence, light at a specific wavelength λ enters the device by a grating coupler. The light intensity is then split equally using a Y-splitter into two waveguides, undergoes phase shift and loss, and is combined additively by a Y-combiner to an output grating coupler where the phase difference determines the output power. The MZI transfer function of the output to input intensity or transmission T_{MZI} for a particular wavelength is

$$T_{MZI}(\lambda) = \frac{I_o}{I_i} = \frac{1}{4} \left| e^{-jB_1(\lambda)L_1} + e^{-jB_2(\lambda)L_2} \right|^2 \quad (1)$$

where $\beta(\lambda)$ is the propagation constant of each arm and is defined as

$$\beta(\lambda) = \frac{2\pi n_{eff}(\lambda)}{\lambda} + j \frac{\alpha}{2} \quad (2)$$

The real component of $\beta(\lambda)$ is the phase term and is dependent on the effective index $n_{\text{eff}}(\lambda)$ of the waveguide. The imaginary component dependent on α represents the optical loss in the waveguide.

One can observe from Eqn. 1 that the phase difference between the two arms can be controlled passively by altering the path length difference $\Delta L = L_2 - L_1$, actively by controlling the effective index, e.g. electro-optic modulation, or both.

Assuming that losses are negligible, the MZI transfer function can be simplified to

$$\frac{I_o}{I_i} = \frac{1}{2}[1 + \cos(\beta_1 L_1 - \beta_2 L_2)] \quad (3)$$

showing that the transmission varies sinusoidally with wavelength through $\beta(\lambda)$.

The free-spectral range (FSR) is the distance between adjacent peaks in wavelength $\Delta\lambda$ or frequency $\Delta\nu$ when plotting the transmission spectrum. The FSR of an imbalanced interferometer for identical waveguides ($n_1 = n_2$) can be expressed as

$$FSR = \Delta\lambda = \frac{\lambda^2}{\Delta L n_g} \quad (4)$$

where the group index n_g for a particular wavelength is defined as

$$n_g(\lambda) = n_{\text{eff}}(\lambda) - \lambda \frac{dn_{\text{eff}}}{d\lambda} \quad (5)$$

The group index n_g is an important parameter since it determines the FSR of an interferometer as shown in Eqn. 4 and is related to the speed at which information travels, i.e. the group velocity v_g :

$$v_g = \frac{c}{n_g} \quad (6)$$

B. Polymer Electro-Optic Modulator Theory

The mechanism behind Polymer electro-optic modulators is Pockel's effect. A material that exhibits Pockel's effect has a refractive index that changes in direct relation to the applied electric field. The change in refractive index of a material due to Pockel's effect is defined as

$$\Delta n = -\frac{1}{2} n_{\text{eop}}^3 r_{33} E \quad (7)$$

where n_{eop} represents the refractive index of the electro-optic polymer, r_{33} is the material's electro-optic coefficient, and E is the applied field [8].

The change in the effective index of the waveguide for a given voltage V or its sensitivity S_p is expressed [9] as

$$S_p = \frac{\partial n_{\text{eff}}}{\partial V_{\text{in}}} = \frac{1}{2} n_{\text{eop}}^3 r_{33} \frac{\Gamma}{d} \quad (8)$$

where Γ is a field confinement factor representing the overlap between electrical and optical fields and d is the distance between the applied signal voltage and ground electrodes [9].

The modulator efficiency, $V\pi L$, is a key characteristic of MZMs where $V\pi$ is the voltage required to add a phase shift of π radians in one of the arms and L is the modulation arm length. A lower modulator efficiency is better as it means less power consumption and physical footprint for the same switching functionality. The $V\pi L$ of the device can be found from the sensitivity S_p using the following formula:

$$V_\pi L = \frac{\pi}{d\beta} = \frac{\lambda}{2 \frac{dn_{\text{eff}}}{dV}} = \frac{\lambda}{2 S_p} \quad (9)$$

Poling is required for the polymer material to have a high r_{33} value as it aligns the chromophore molecules towards the direction of the poling electric field. This procedure is illustrated in Fig. 2. The r_{33} value is approximately linear to the poling field as shown in Fig. 3 for a 2:1 HLD1/HLD2 (wt/wt) polymer.

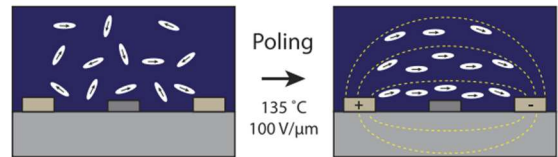


Figure 2. Poling procedure of chromophore molecules in a polymer [10].

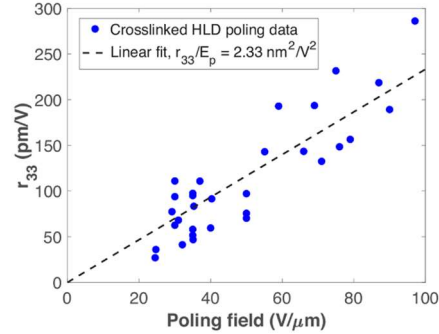


Figure 3. Electro-optic activity of cross-linked HLD (2:1 HLD1/HLD2) exhibits linear behaviour [11].

C. Simulations

From Eqn. 1, one can simulate the transmission spectrum $T_{\text{MZI}}(\lambda)$ of a Mach-Zehnder interferometer with known optical path lengths L_1 and L_2 if the $n_{\text{eff}}(\lambda)$ of the two waveguides can be acquired.

Lumerical MODE Solutions was used to extract the effective indices of a waveguide accounting for both waveguide and material dispersion. A layout was created in Lumerical MODE to simulate a 220 nm thick, 500 nm Silicon waveguide on buried oxide (BOX) with different cladding as shown in Figure 4.

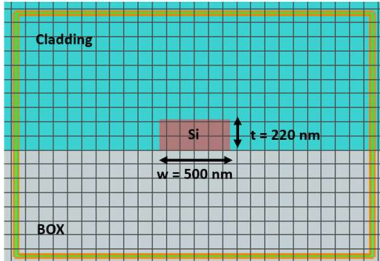


Figure 4. Lumerical MODE layout for extracting effective indices of a Silicon waveguide on SOI wafer with different cladding.

Simulations were performed with a cladding of air and HLD1/HLD2 polymer to compare with the optical measurements. Air was chosen to have a fixed refractive index of 1.0003. The HLD1/HLD2 polymer was chosen to have a fixed refractive index of 1.83 with cross-linking [12]. The mode profiles are shown in Fig. 5.

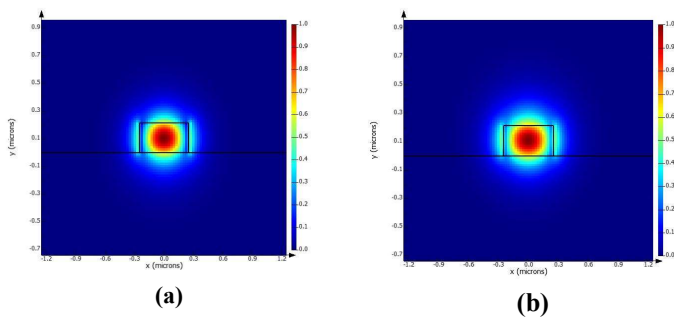


Figure 5. Ex mode profiles for the fundamental quasi-TE polarized light ($\lambda=1.55 \text{ } \mu\text{m}$) calculated using Lumerical MODE. (a) Air cladding ($n=1.0003$). (b) HLD1/HLD2 cladding ($n=1.83$). More light is present in the polymer cladding due to the smaller index difference between core and cladding.

The results of the wavelength sweep simulations were extracted to model the waveguide in MATLAB. A 2nd order Taylor series polynomial around the centre wavelength $\lambda_0 = 1550 \text{ nm}$ (Eqn. 10) was used to model the effective index behaviour (Fig. 6). The group index was also modelled (Fig. 7).

$$n_{\text{eff}}(\lambda) = n_1 + n_2(\lambda - \lambda_0) + n_3(\lambda - \lambda_0)^2 \quad (10)$$

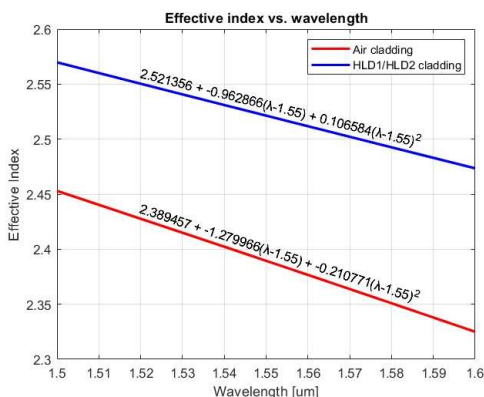


Figure 6. Effective index vs. wavelength of air and polymer cladding using 2nd order Taylor series model. Average effective index: $n_{\text{eff,air_clad}} = 2.389277$, $n_{\text{eff,EOP_clad}} = 2.521446$.

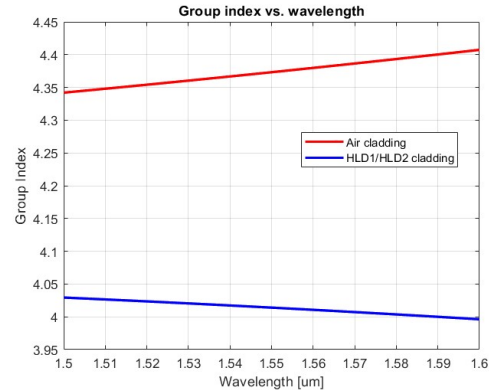


Figure 7. Group index vs. wavelength for air and polymer cladding. Average group index: $n_{g,\text{air_clad}} = 4.373676$, $n_{g,\text{EOP_clad}} = 4.013612$.

The transmission spectrum of the MZI (Fig. 8) was then modelled for both cladding materials using Eqn. 1 given that both waveguides have the same effective index. The path length difference ΔL was set to 431.67 microns to replicate the designed MZI for future comparison. The loss coefficient α was set to zero to visualize the general behaviour.

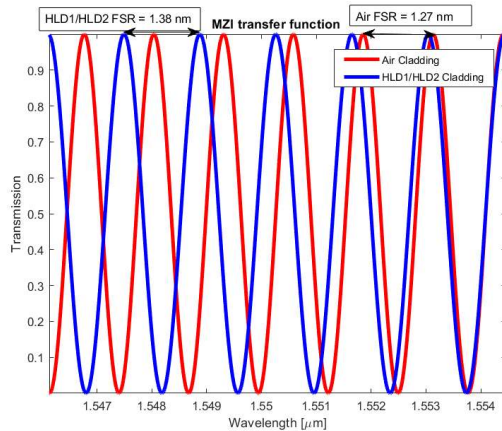


Figure 8. Transmission vs. wavelength of a lossless, imbalanced MZI with air and polymer cladding. $\Delta L = 431.67$ microns. The FSR of air is smaller since the group index is larger from Fig. 7.

Lastly, simulations of the electro-optic effect were performed. Higher electrical-optical field interaction Γ in the cladding material was seen in simulations of a slot waveguide geometry (Fig. 9) compared to a strip waveguide geometry (Fig. 10) which results in better modulation efficiency or lower $V\pi L$.

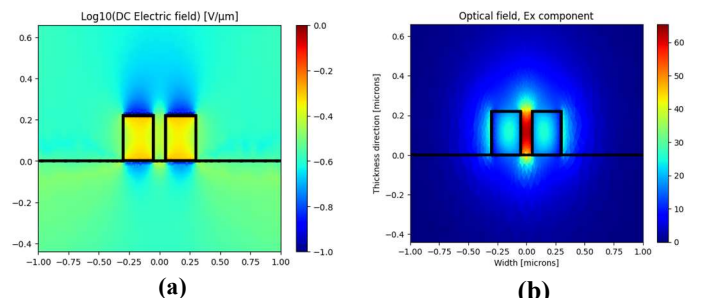


Figure 9. Electrical (a) and optical field (b) simulations for a slot waveguide.

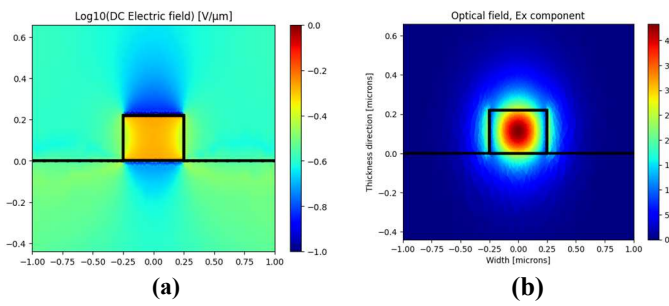


Figure 10. Electrical (a) and optical field (b) simulations for a strip waveguide.

The effective index vs. voltage (Fig. 11) for $\lambda = 1550$ nm was simulated from the effective index model of the polymer-clad waveguide produced in Fig. 6 and calculating from Eqn. 8 the sensitivity S_p of the electro-optic modulator. The field confinement factor of the cladding Γ was estimated to be 0.14 from Appendix A for a waveguide width of 500 nm. The refractive index n_{eop} of HLD1/HLD2 polymer cross-linked is 1.83 [12]. The electro-optic coefficient r_{33} was estimated to be 23 pm/V assuming a poling voltage of 210 V and poling electrode distance of 22 microns producing a poling field $E = 9.55$ V/ μm [12, Fig. 7h]. The signal electrode distance d is 8.49 microns from a KLayout design.

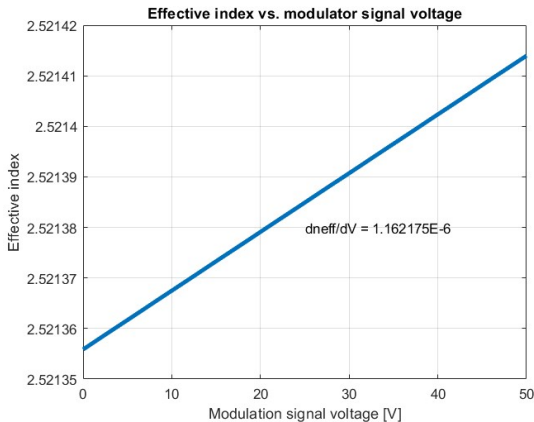


Figure 11. Effective Index vs. modulation signal voltage for $\lambda = 1550$ nm. Parameters: $n_{eop} = 1.83$, $\Gamma = 0.14$, $r_{33} = 23$ pm/V, $d_{signal} = 8.49$ microns. Calculated sensitivity $d\text{neff}/dV = 1.1622\text{E-}6$ V $^{-1}$.

The transmission spectrum was then simulated to include modulation based on the calculated sensitivity. To compare with future experimental results, voltage is applied for a modulation arm length $L_{mod} = 3000$ μm for one arm (Fig. 12) and both arms (Fig. 13) in a push-pull configuration [13]. The spatial phase shift experienced in each arm is defined as

$$\theta = \frac{2\pi n_{eff}}{\lambda} L_{nomod} + \frac{2\pi(n_{eff} + \frac{\partial n_{eff}}{\partial V} V)}{\lambda} L_{mod} \quad (11)$$

where the total arm length is $L_{nomod} + L_{mod}$.

A push-pull configuration results in a more efficient modulator since the light in the two arms experience phase shifts in opposite direction [14], effectively halving the $V_\pi L$ FoM. This can be confirmed by comparing Figures 12 and 13.

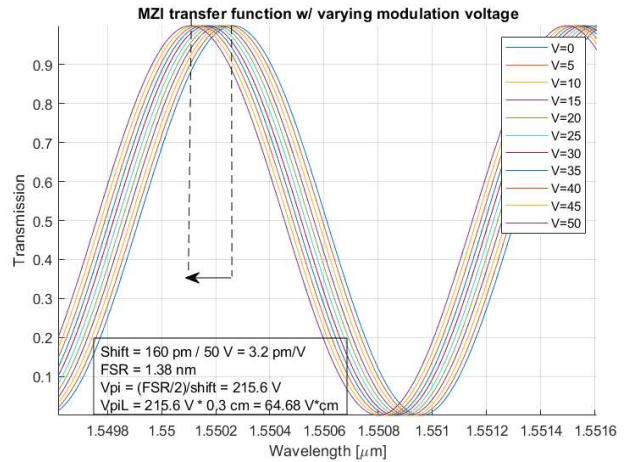


Figure 12. Simulated MZM transmission vs. wavelength with varying modulation voltages on one arm with polymer cladding. Parameters: $L_{1,mod} = 3$ mm, $L_{1,nomod} = 278$ μm , $L_{2,nomod} = 3.8$ mm.

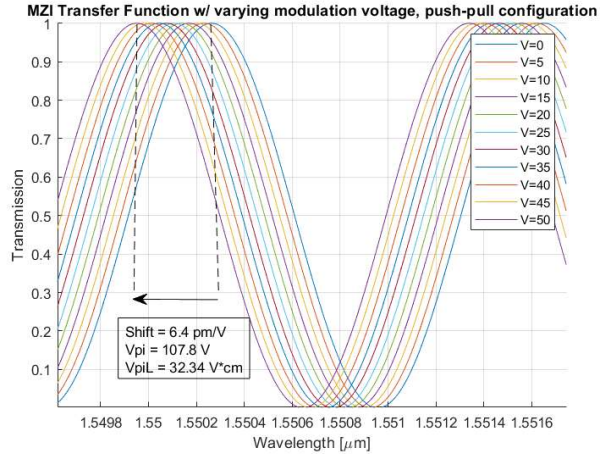


Figure 13. Simulated MZM transmission vs. wavelength with varying modulation voltages in a push-pull configuration. Parameters: $L_{1,mod} = L_{2,mod} = 3$ mm, $L_{1,nomod} = 278$ μm , $L_{2,nomod} = 709$ μm .

III. DESIGN

A. Design Objective

The main objective of the modulator designs was to minimize the half-wave voltage V_π figure of merit to minimize power consumption. The secondary objective was to observe how varying modulation arm length would affect the device's $V_\pi L$ product as described in Section II-B.

B. Design Approach

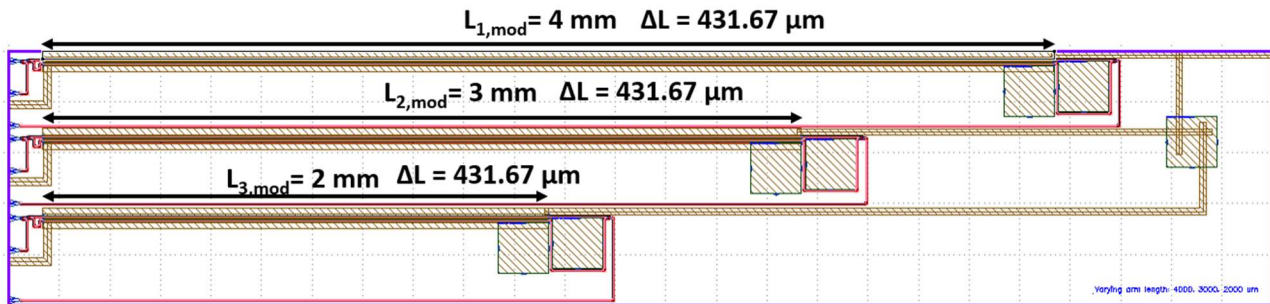


Figure 14. Electro-optic phase shifter layout using KLayout for 3 devices with different modulation length $L_{x,\text{mod}}$.

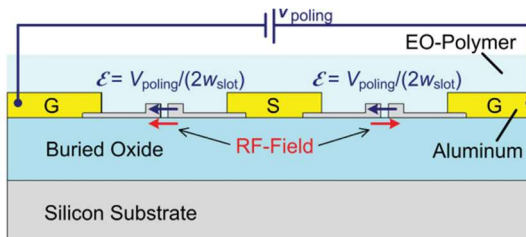


Figure 15. Cross-section of a polymer modulator employing a push-pull architecture [15].

The design layout of 3 electro-optic MZMs of varying modulation length is shown in Figure 14. A push-pull MZM configuration like Figure 15 was employed since simulations in Section II showed that it effectively doubled the modulator response. In essence, this is because the poling field aligns the chromophores in each waveguide in one direction. The RF (signal) field, however, opposes the poling field in the right waveguide and vice-versa for the left waveguide. This causes phase shift in opposite directions between the two waveguides minimizing V_π .

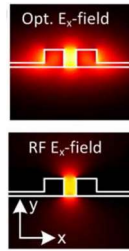


Figure 16. Cross-section of strip-loaded slot waveguided with optical and RF fields colour-coded [16].

The optical-electrical field overlap Γ directly related to the device's sensitivity $d\eta_{\text{eff}}/dV$ can be maximized by using strip-loaded slot waveguides as shown in Figure 16. The overlap is about five times compared to traditional strip waveguides [17]. The actual design, however, uses strip waveguides since it was offered as a parameterized cell (PCell) by the SiEPIC Program EBeam PDK for the ZEP process [18] to minimize risk of failure at the expense of higher V_π .

The poling field can be maximized to increase the r_{33} of the electro-optic material by minimizing the gap between the poling electrodes. The poling electrode distance $d_{\text{poling}} = 22 \mu\text{m}$ as shown in Fig. 17 was limited by the design rules for the process (Appendix A), namely the minimum Si-Metal exclusion of 4 μm and the minimum Metal feature size of 5

μm . A poling voltage of 210 V produces a poling electric field $E_{\text{poling}} = 210 \text{ V}/22 \mu\text{m} = 9.55 \text{ V}/\mu\text{m}$.

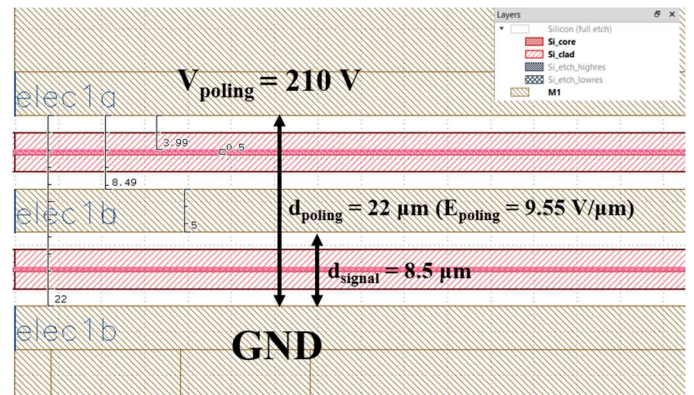


Figure 17. Top-down view of push-pull EO phase shifter in KLayout.

The signal electrode distance $d_{\text{signal}} = 8.5 \mu\text{m}$ was also minimized to increase $d\eta_{\text{eff}}/dV$ from Eqn. 8. This distance too was limited by the design rules for the process.

Lastly, each student was allocated a design area of 5000 $\mu\text{m} \times 1000 \mu\text{m}$ on the chip. The full design area width was utilized to maximize the modulation arm length L_{mod} and thus maximize the phase shift along the waveguides for a given signal voltage since $\theta = \text{Re}(\beta)*L$. This lowers V_π at the expense of increased optical propagation loss due to higher waveguide lengths.

C. Design of Experiment

The parameter varied in the designs was the modulation arm length L_{mod} as listed in Table 1. This parameter was varied to observe a fundamental operating principle that a smaller L_{mod} requires a larger V_π .

Design #	Modulation Arm Length (L_{mod})
1	4000 μm
2	3000 μm
3	2000 μm

Table 1 – Design parameters for the Mach-Zehnder Interferometer Electro-Optic Phase shifter.

D. Additional Mask Layout Details

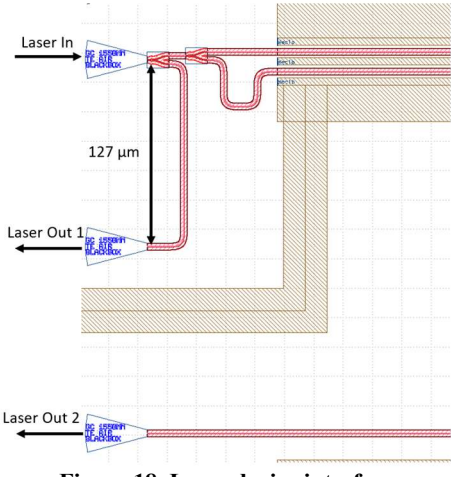


Figure 18. Laser device interface.

Figure 18 shows the external laser to device interface for a single device. The surface grating couplers were spaced 127 μm apart and faced right to be compatible with UBC's automated probe station. The first Y-splitter splits half the input light intensity to output 1 as a method of de-embedding the bandwidth and insertion loss of the grating couplers from the transmission spectrum. The second Y-splitter splits light into the push-pull EO MZM. The additional length in the lower waveguide entering the modulator was required to accommodate the minimum TE bend radius rule of 5 μm required to minimize loss. Laser output 2 is the output of the MZM. The top and bottom metal electrodes were connected to one of the global rails (210 V or GND) outside the designated design area for poling.

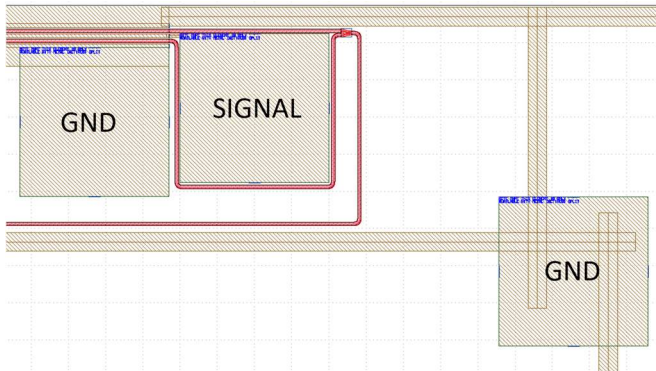


Figure 19. Electrical bond pads.

Wire-bonding to an external PCB was chosen as the interface for electrical testing. The positioning of the 200x200 μm bond pads are shown in Figure 19. The signal bond pad was required to be placed between the two waveguides since the process was limited to a single metal layer. The signal bond pad placement indirectly creates additional path length difference between the two waveguides increasing the frequency of the sinusoidal transmission spectrums. One outer electrode of each device is connected to a global GND pad to save on material and cost since gold was to be used for the metal layer.

IV. EXPERIMENTS

A. Fabrication

The SOI wafer used had a Si substrate thickness of 725 μm , a buried oxide (BOX) thickness of 3500 nm, and a top Si thickness of 220 nm. The wafer is diced into four 12x12 mm chips to create four copies of the devices for testing.

1) ZEP Resist Spin Coat

The chips were first spun-coat with ZEP520A-7, a positive resist compatible with electron-beam lithography (EBL). Prior to spin-coating, the chips were cleaned with Acetone and IPA for two minutes in an ultra-sonic bath and then dried using a nitrogen N₂ gun. They then underwent oxygen plasma cleaning using a Plasma-Etch PE-50 for 30 seconds at 20 SCCM to increase surface hydrophilicity/wettability. The chips were hot-baked at 180°C for 10 minutes to remove water vapour. The resist was dispensed onto the wafer. The spin-coat recipe is to first accelerate at 200 rpm/s and hold at 500 rpm for 3 seconds to spread the resist. Then, accelerate at 1000 rpm/s to 2000 rpm and hold for 35 s to obtain an appropriate resist thickness. The chips were then baked once more at 180°C for 1 minute to adequately solidify the resist by evaporating the solvent. The measured resist thickness was 260 nm.

2) Electron Beam Lithography



Figure 20. JEOL JBX-8100FS Electron-beam column image taken by Neal, a student in the 2023 cohort.

The first Silicon layer was patterned using electron beam lithography with the JEOL JBX-8100FS system. BEAMER software licensed by Genisys GmbH was used to convert the output GDS pattern files from KLayout into J52 format compatible with the E-beam system. The BEAMER software also performed proximity correction: computing the optimum exposure dosage around the pattern based on electron scattering effects, primarily back-scattering [18]. The resist-coated chips were placed onto a cassette and then loaded into the electron beam column as shown in Figure 20. The operating parameters included a base dosage of 213 $\mu\text{C}/\text{cm}^2$, a shot pitch of 4 nm, a current of 1 nA, and a voltage of 100 kV. After exposure, the positive resist is developed using ZED-N50 for 1 minute removing the exposed area. Lastly, the device is cleaned and dried using IPA and N₂, respectively. Figure 21 shows a post-development optical image where the exposed Silicon area around the waveguide is visible.

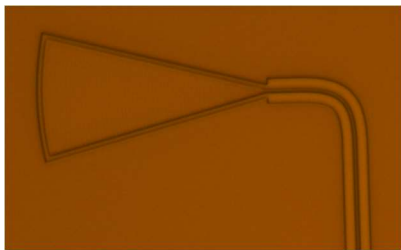


Figure 21. Silicon mask post-development optical microscope image taken by Sheri Chowdhury, a course TA.

3) Plasma Etch

The exposed silicon was plasma-etched in reactive ion etching (RIE) mode to enhance directionality, using the Oxford PlasmaPro 100 Cobra tool. The recipe involved maintaining a temperature of 15°C, a pressure of 10 mTorr, an etch time of 3 minutes and 30 seconds, 25 sccm of SF₆, 35 sccm of C₄F₈, HF power at 30W, ICP forward power at 600W, and a DC bias of 220V. Following the etching process, the wafers were placed in a UV chamber for 15 minutes to denature the links in the remaining resist. Subsequently, they were dipped into a MICROPOSIT Remover 1165 solution to strip the resist from the substrate. Figure 22 displays an optical image of the chip after silicon etching and resist removal, with the darker region indicating the visible BOX layer post-etch.

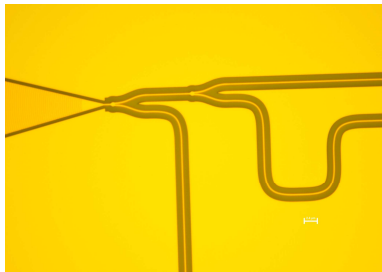


Figure 22. Post silicon etch optical image.

4) Metal Deposition

The metal layer is applied using the lift-off technique. An image reversal photoresist named AZ-5124E-IR was used for the mask since it produces a negative side-wall profile suitable for lift-off [20] and because negative resists are difficult to procure. Figure 23 illustrates the general procedure for image reversal that was followed. For brevity, the reader can refer to the SQBMI Advanced Nanofabrication Facility website for the photoresist recipe [22]. The patterning was performed using a MLA150 maskless optical lithography system.

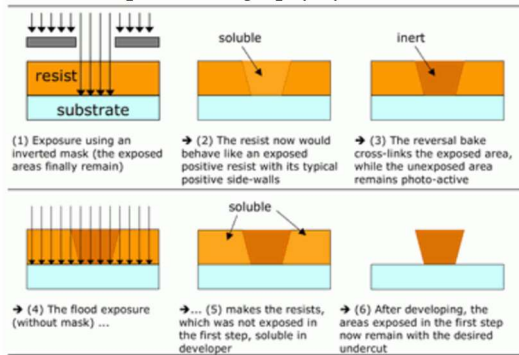


Figure 23. Image reversal procedure for AZ 5124E-IR [21].

After development and cleaning, physical vapor deposition (PVD) of the metal layer was performed using UBC's custom-built electron beam evaporator named DeeDirectors. A 5 nm layer of titanium (Ti) was first deposited to act as an adhesion layer, followed by the deposition of a 100 nm layer of gold (Au). The metal deposited on the remaining resist is then lifted off together using Microposit Remover 1165 to remove the bulk of the photoresist. A second bath is performed using Acetone in a heated ultrasonic cleaner at 60°C for 4 minutes to remove any remaining traces of photoresist. The result is shown in Figure 24.

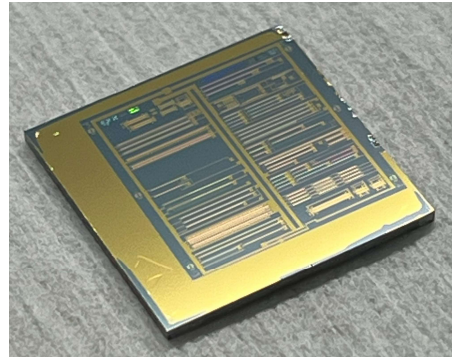


Figure 24. Chip after deposition of the metal layer.

5) Polymer Deposition

A 2:1 HLD1:HLD2 (wt/wt) chromophore polymer film was deposited onto the chips to provide electro-optic modulation. 45 mg of HLD1 and 23 mg of HLD2 was dissolved into 687 mg or 0.48 mL of 1,1,2-trichloroethane (TCE) solvent using an ultrasonic bath for 30 minutes to create a 9 wt% solution that will produce a ~1-1.5 μm thick film post-spin. The solution was then spun coat onto the devices at 500 rpm for 5 seconds, 850 rpm for 30 seconds, and then 1500 rpm for 30 seconds.

6) Poling/Cross-linking

Lastly, the polymer material was electrically poled to provide a high Pockel's coefficient r_{33} and thermally cross-linked for long-term stability. The devices were placed in a chamber purged with Nitrogen gas to minimize oxidation of the polymer. Due to low resistivity between the global poling rails, the poling voltage of 210 V was only applied to a small number of devices using an electrode not connected to the global rail. The chips were then heated in 10°C steps from 95°C to 155°C, holding at each temperature for 10 minutes before cooling to room temperature and then turning off the poling field. The leakage current between the poling rails was measured during the entire process to ensure that the poling and crosslinking reactions were taking place as shown in Figure 25. A cross-sectional summary of the fabrication steps is illustrated in Figure 26.

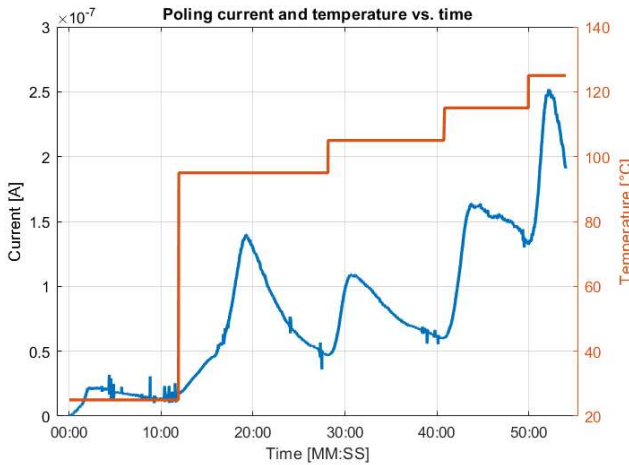


Figure 25. Poling current and temperature vs. time for Thursday's lab section. Note that temperature was deduced from the measured current and does not include rise time. Poling increases with temperature leading to higher conductance. Resistivity of film increases when temperature is held due to cross-linking [23].

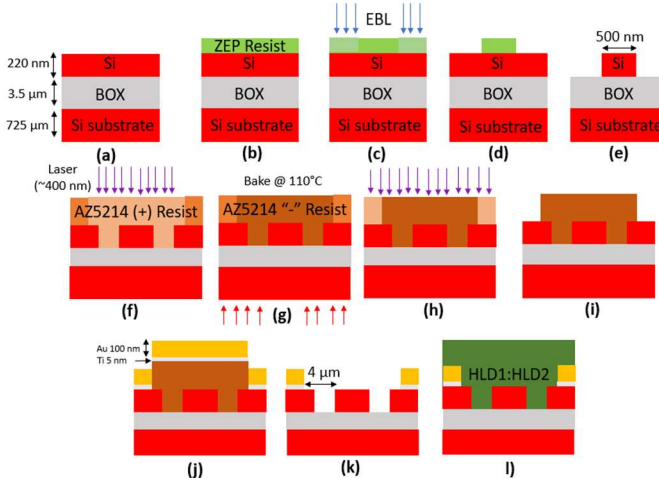


Figure 26. Fabrication cross-section summary. (a) Initial wafer (b) ZEP resist spin coat (c) EBL (d) Develop (e) Plasma etch (f) Image reversal resist spin coat, first exposure (g) Bake to create "-" resist (h) Flood exposure (i) Develop (j) PVD of metals (k) Lift-off (l) Polymer application, poling, cross-linking

B. Test Methodology

To characterize the devices, a custom-built automated test setup [24] with automated control software written in Python was used [25]. An Agilent 81600B tunable laser was used as the input source and Agilent 81635A optical power sensors as the output detectors. The wavelength was swept from 1500 to 1600 nm in 10 pm steps. A polarization maintaining (PM) fibre was used to maintain the polarization state of the light, to couple the TE polarization into the grating couplers [26]. A polarization maintaining fibre array was used to couple light in/out of the chip [27].

Optical measurements were taken after the etching of Silicon to characterize the performance of the passive MZMs. Measurements were taken for all four chips to analyze for process variability. Optical measurements were also taken after the deposition and poling of the polymer to test the

behaviour of the active electro-optic MZMs. The modulation voltage was applied in increments, both positive and negative, to observe shifts in the transmission spectrum as expected from simulations.

C. Results

Active measurements were performed for one device labelled "timbitss_polymod2" (the middle device in Figure 14) with modulator length $L_{\text{mod}} = 3 \text{ mm}$ and $\Delta L = 431.67 \mu\text{m}$. Plots of the raw transmission spectrum for varying wavelengths are shown for positive modulation voltages (Figure 27) and negative modulation voltages (Figure 28) between 0-10 V for the second push-pull device in Figure 14 labelled. The center (peak) wavelength $\lambda_o = 1.5276 \mu\text{m}$ was acquired from by locating the maximum of the loopback response.

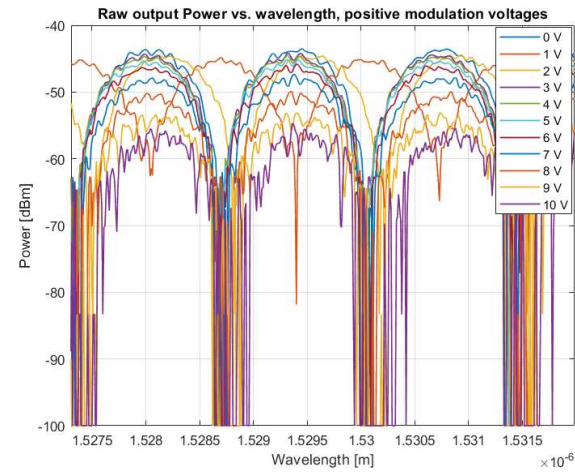


Figure 27. Raw output power vs. wavelength data for positive DC modulation voltages (12/06/2023).

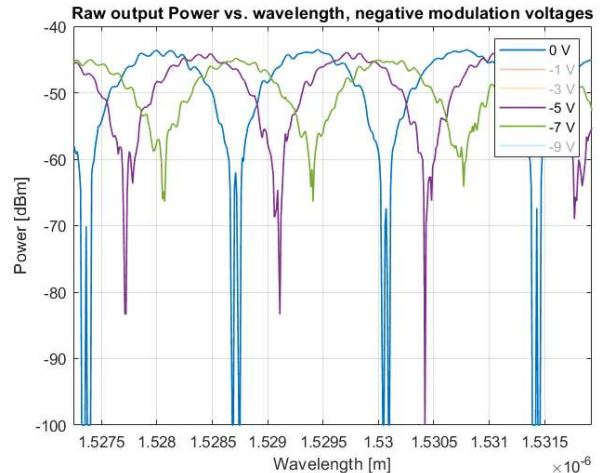


Figure 28. Raw output power vs. wavelength data for negative DC modulation voltages (12/06/2023). The spectrum shifts right with decreasing voltage.

Measurements of the air-clad passive devices were also taken prior to polymer deposition.

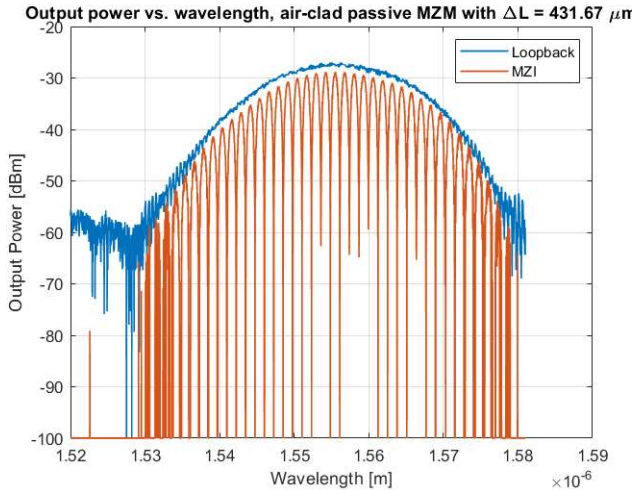


Figure 29. Output power vs. wavelength for air-clad passive MZM (chip4, timbitss_polymod2). Path length difference $\Delta L = 431.67 \mu\text{m}$.

V. ANALYSIS

The negative voltage modulation data was used for subsequent analysis since positive modulation voltages from Fig. 27 by visual inspection exhibited zero shift overall.

The loopback response (output 1 in Fig. 18) was subtracted from the MZM transmission spectrum at each voltage to remove the Gaussian-like effect of the bandwidth-limited grating couplers and then Gaussian-smoothed for easier characterization. The processed data is shown in Figure 30.

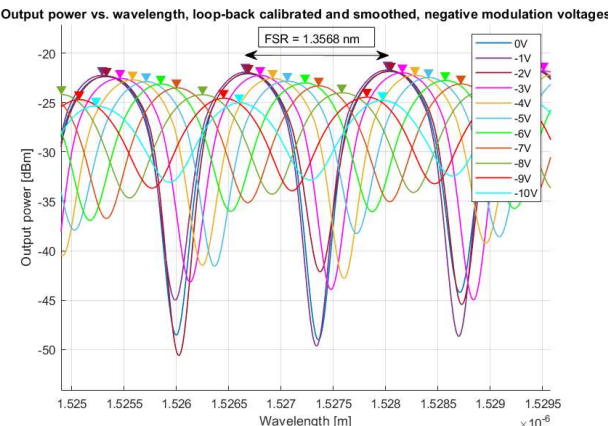


Figure 30. Output power vs. wavelength with loop-back calibration and smoothing applied. $\text{FSR}_{\text{average}} = 1.3568 \text{ nm}$.

The peak wavelength phase shift $\Delta\lambda$ with applied voltage was extracted from Figure 29 and is displayed in Figure 31. A straight-line fit was applied assuming that the phase shift was approximately linear with voltage starting from -2 V. The half-wave voltage $V_\pi = 6.569 \text{ V}$ was obtained from the curve fit.

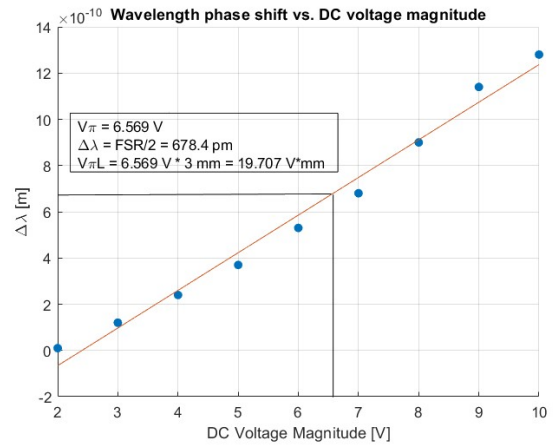


Figure 31. Wavelength phase shift vs. DC voltage magnitude with straight-line fit. $V_\pi = 6.569 \text{ V}$ for $\Delta\lambda = \text{FSR}/2 = 678.4 \text{ pm}$. $V_\pi L = 19.707 \text{ Vmm}$.

The EO coefficient $r_{33} = 767 \text{ pm/V}$ was obtained from the measured half-wave voltage $V_\pi = 6.569 \text{ V}$ using Eqn. 8 and 9. The simulated r_{33} and FSR values were re-calculated for a new central wavelength $\lambda_0 = 1.5276 \mu\text{m}$ and poling distance of 8.5 μm . The simulated and experimental results for the active MZM are compared in Table 2.

Table 2. Comparison of simulated and experimental parameters for active EO polymer MZM (timbitss_polymod2).

Parameter	Simulated	Experimental	Abs. Error [%]
FSR [m]	1.3444E-9	1.3568E-9	0.92
$V_\pi [\text{V}]$	87.537	6.569	92.5
$r_{33} [\text{pm/V}]$	57.56	767	1232

The experimental data from applying 0 V to the EO polymer MZM (passive operation) was loop-back calibrated and then modelled using the transfer function

$$T_{\text{MZI}}(\lambda) = 10 \log_{10} \left(\frac{1}{4} \left| 1 + e^{\frac{2\pi n_{\text{eff}}(\lambda)}{\lambda} \Delta L - \frac{\alpha \Delta L}{2}} \right|^2 \right) + b \quad (12)$$

where $n_{\text{eff}}(\lambda)$ is a second order Taylor series model (Eqn. 10). The five model fit parameters are n_1 , n_2 , n_3 , α , and b representing the excess loss of the MZM. After successful curve-fitting (Fig. 32), the group indices $n_g(\lambda)$ were obtained using Eqn. 5 and the effective index coefficients. The experimental data was then compared with the Lumerical MODE simulation data as shown in Figure 33 and Table 3. The same procedure was performed for the air-clad device data with results shown in Figure 34 and Table 4.

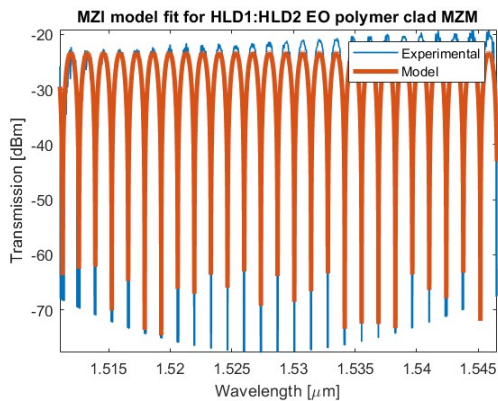


Figure 32. Model fit for HLD1:HLD2 EO polymer clad MZM using autocorrelation. Fit parameters: $n_1 = 2.402767$, $n_2 = -1.037708$, $n_3 = -0.057858$, $\alpha = 1.717831E-5$, $b = -23.275068$. $\lambda_o = 1.5288 \mu m$.

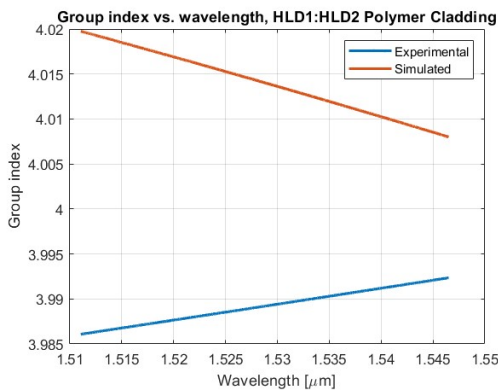


Figure 33. Group index vs. wavelength for HLD1:HLD2 Polymer cladding from experimental data and Lumerical MODE 2D waveguide simulations.

Table 3. Comparison of simulated and experimental parameters for a passive HLD1:HLD2 EO MZM, $\lambda_o = 1.5288 \mu m$.

Parameter	Simulated	Experimental	Absolute Error [%]
n_{eff}	2.541816	2.402767	5.4704
n_g	4.014022	3.989195	0.6185

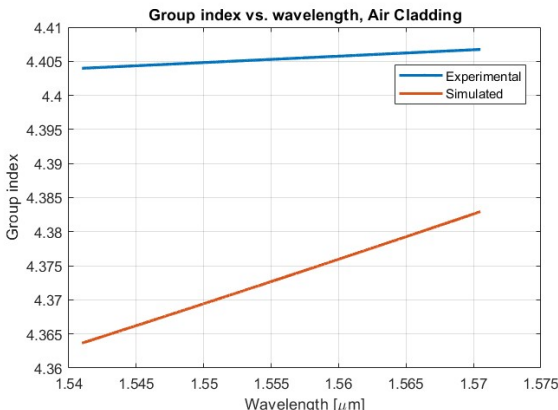


Figure 34. Group index vs. wavelength for air cladding from experimental data and Lumerical MODE 2D waveguide simulations.

Table 4. Comparison of simulated and experimental parameters for air-clad passive MZI, $\lambda_o = 1.5557 \mu m$.

Parameter	Simulated	Experimental	Absolute Error [%]
n_{eff}	2.382153	2.403119	0.8801
n_g	4.373143	4.398059	0.5698

VI. DISCUSSION

As shown in Table 2, the performance of the EOP modulator far exceeded expectations from comparing the extracted versus simulated V_π and r_{33} . The large error may have been due to inadequate estimation of values for the dn_{eff}/dV expression (Eqn. 8). The error was minimized by adjusting the field overlap factor $\Gamma = 1$, $n_{cop} = 1.88$ at $\lambda = 1550\text{nm}$, and $r_{33} = 3.23 \text{ nm}^2/\text{V} * 210 \text{ V} / 8.5 \mu m = 79.8 \text{ pm/V}$ assuming no cross-linking [23]. This adjustment produced a “best-case” simulated $V_\pi = 8.153 \text{ V}$ and experimental $r_{33} = 99 \text{ pm/V}$ calculated from Eqns. 8 and 9, but it relies on parameter overestimation.

A possible solution to improving the accuracy and estimated parameters n_{cop} and r_{33} s by automating the process of preparing the HLD solution using a robotic system. Since students were asked to prepare the HLD solution by hand, the error in chromophore concentration can lead to under or overestimation of the r_{33} and n_{cop} , and hence V_π . Automation of this step would also lower variability between chips.

Many devices were unable to be poled because of a low measured resistance between the global poling rails connected to each device. The low resistance may be attributed to metal residue remaining between the metal tracks, which the lift-off process could not remove. Additionally, there could be excess silicon that was not removed fully by the plasma etching process.

Ultimately, the poling roadblock reduced the device yield available for testing to only five. Since a desired outcome for the course is to allow students to test and validate their own designs, improving the yield should be a goal for future cohorts. A suggestion would be to localize poling to individual sections of the chip such that a short does not affect all the devices. In addition, adding multiple test points around the chip at the global rails would help to identify the source of the short. Another suggestion would be to add jumpers between sections of the global rails so that the area containing the short can be isolated from the rest of the chip.

VII. CONCLUSION

The tested HLD1:HLD2 EO polymer modulator exhibited a half-wave $V_\pi = 6.569$ and $V_\pi L = 19.707 \text{ Vmm}$ indicating that SOH modulators can match the performance of FCD modulators produced in CMOS foundries today. However, more robust methods of preparing the electro-optic material and poling of multiple devices on a single chip must be investigated before SOH modulators can be integrated reliably into existing Si platforms. Suggested future research topics include automated preparation of EO material using robotic systems and strategies for mitigating electrical shorts in a global poling chip layout topology.

ACKNOWLEDGEMENT

I acknowledge the edX UBCx Silicon Photonics Design, Fabrication and Data Analysis course, which is supported by the Natural Sciences and Engineering Research Council of Canada (NSERC) Silicon Electronic-Photonic Integrated Circuits (SiEPIC) Program. The devices were fabricated by Sheri Chowdhury and Iman Taghavi at the UBC Nanofabrication facility. Iman Taghavi performed the measurements at The University of British Columbia. We acknowledge Lumerical Solutions, Inc., Mathworks, Python, and KLayout for the design software. Lastly, I would like to thank Dr. Chrostowski for the conception of this insightful introductory course in nanofabrication.

REFERENCES

- [1] <https://ece.ubc.ca/courses/elec-463/>
- [2] Silicon Photonics Design From Devices to Systems Lukas Chrostowski, Michael Hochberg
- [3] Polymer modulators in silicon photonics: review and projections
- [4] A 128 Gb/s PAM4 Silicon Microring Modulator
- [5] 100 GHz silicon–organic hybrid modulator
- [6] Nonlinear polymer-clad silicon slot waveguide modulator with a half wave voltage of 0.25 V
- [7] Recent advances in polymer electro-optic modulators
- [8] Silicon-on-Insulator Slot Waveguides: Theory and Applications in Electro-Optics and Optical Sensing pp.201
- [9] I. Taghavi et al.: Polymer modulators in silicon photonics section 2.2
- [10] Witmer_2020_Quantum_Sci._Technol._5_034004.pdf pg. 5
- [11] <https://www.nlmphotonics.com/technology/products/>
- [12] Ultrahigh Electro-Optic Coefficients, High Index of Refraction, and Long-Term Stability from Diels–Alder Cross-Linkable Binary Molecular Glasses Section 2.5
- [13] Low Power Mach-Zehnder Modulator in Silicon-Organic Hybrid Technology Fig. 1d
- [14] Electro-Optic Organic Crystal Silicon High-Speed Modulator Sec. 2
- [15] Low Power Mach-Zehnder Modulator in Silicon-Organic Hybrid Technology Fig. 1d
- [16] Electro-Optic Organic Crystal Silicon High-Speed Modulator Fig. 1
- [17] Silicon-on-Insulator Slot Waveguides: Theory and Applications in Electro-Optics and Optical Sensing Sec. 2.4
- [18] https://ebeam.wnf.uw.edu/ebeamweb/doc/patternprep/patternprep/proximity_main.html
- [19] https://www.microchemicals.com/products/photoresists/az_5214_e.html
- [20] https://www.microchemicals.com/micro/tds_az_5214e_photoresist.pdf
- [21] https://www.microchemicals.com/nc/products/photoresists/lift_off_resistsnegative_resists.html
- [22] https://www.nanofab.ubc.ca/processes/photolithography/az_5214e-ir-positive-and-image-reversal-photoresist/
- [23] Ultrahigh Electro-Optic Coefficients, High Index of Refraction, and Long-Term Stability from Diels–Alder Cross-Linkable Binary Molecular Glasses
- [24] Lukas Chrostowski, Michael Hochberg, chapter 12 in "Silicon Photonics Design: From Devices to Systems", Cambridge University Press, 2015
- [25] <http://siepic.ubc.ca/probestation>, using Python code developed by Michael Caverley.
- [26] Yun Wang, Xu Wang, Jonas Flueckiger, Han Yun, Wei Shi, Richard Bojko, Nicolas A. F. Jaeger, Lukas Chrostowski, "Focusing sub-wavelength grating couplers with low back reflections for rapid prototyping of silicon photonic circuits", Optics Express Vol. 22, Issue 17, pp. 20652-20662 (2014) doi: 10.1364/OE.22.020652
- [27] www.pleconnections.com, PLC Connections, Columbus, OH.

VIII. APPENDIX

A. SiEPICfab-EBeam-ZEP-PDK Design Rules

Table 4. Minimum Feature Size

Layer	Minimum Feature Size	Overlay Accuracy
Si	80 nm	N/A
Metal	5 μm	3 μm

Table 5. Minimum Space Between Layers

Layer	Si	Metal
Si	80 nm	4 μm
Metal	-	5 μm

B. Miscellaneous Lab Photos

Figure 35. HLD1 and HLD2 material placed in separate vials in a 2:1 weight ratio (45 mg : 23 mg) prior to dissolving with 1,1,2-trichloroethane (TCE).



Figure 36. HLD1:HLD2 chromophore solution using TCE solvent with approximately 9 wt% solution of chromophore.

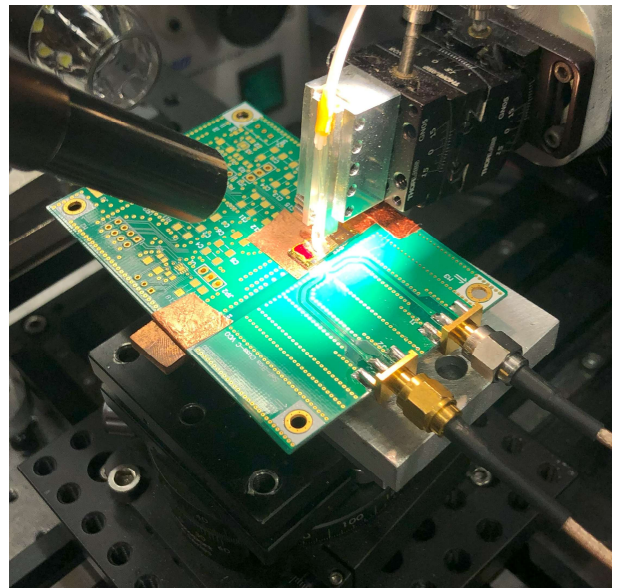


Figure 37. Automated optical probe station taking measurements.

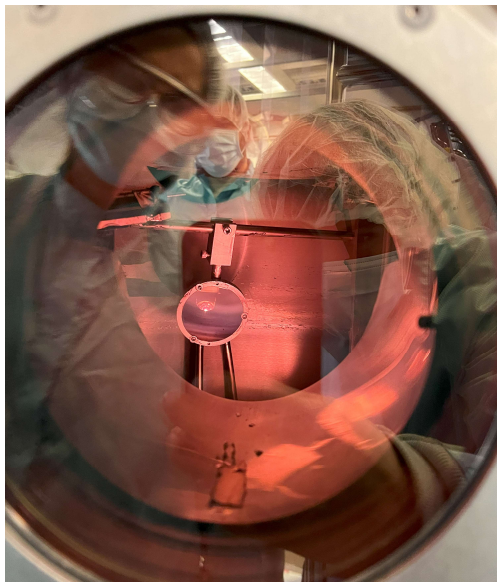


Figure 38. Inside view of DEEDIRECTORS-2015: 8 source load-lock electron beam evaporator where crucible containing gold is evaporated using electron beam heating.

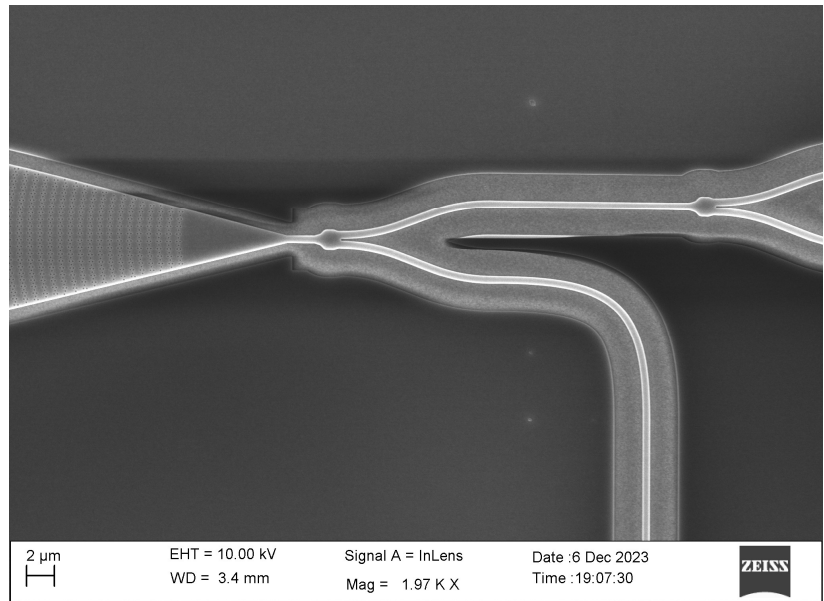


Figure 39. SEM image of chip taken by Sheri Chowdhury after Silicon etching showing the grating coupler and two Y-splitters.

C. MATLAB code for plotting n_{eff} vs. voltage and MZI transmission spectrums with varying modulation voltages

```
% Load 2nd order polynomial coefficients n1, n2, n3 for effective index
% model of the polymer-clad waveguide
polymer = load("data\n_eff_vs_wavelength_coeffs_polymer_cladding.mat")
lambda0 = 1.55

% Use anonymous function the effective index expression
neff_eq = @(nx, lambda) (nx(1) + nx(2).*(lambda-lambda0) + nx(3).*(lambda-lambda0).^2);

%% Plot effective index vs. voltage for a particular wavelength
lambda = 1.55 % Wavelength of interest [um]
```

```

neop = 1.83 % Electro-optic polymer index of refraction
r33 = 23e-12 % Electro-optic coefficient obtained from r33 vs. poling field
overlap_factor = 0.14 % Electrical-optical field overlap factor
d = 8.49e-6

% Calculate modulator sensitivity (Sp = dneff/dV)
sp = (0.5*neop^3*r33*overlap_factor/d)

% Effective index at 0 V is simply obtained from the waveguide model
neff_0V = neff_eq(polymer.X, lambda)

% neff(V) = neff_0V + dneff/dV*V
neff_vs_v_eqn = @(V) (neff_0V + sp*V)

% Plot neff vs. voltage
min_voltage = 0
step = 5
max_voltage = 50
voltages = min_voltage:step:max_voltage
plot(voltages, neff_vs_v_eqn(voltages), "LineWidth", 3)
grid on;
xlabel("Modulation signal voltage [V]")
ylabel("Effective index")
title("Effective index vs. modulator signal voltage")

% Place slope on graph
text(mean(voltages), neff_vs_v_eqn(mean(voltages))-5E-6, sprintf("dneff/dV = %fE-6", sp*1e6))

%% Acquire transmission (Output intensity/Input intensity) vs. wavelength
% Equal waveguide: B1 = B2 = B = 2*pi*n_eff(lambda)/lambda
% Unbalanced lengths: L1 != L2
alpha = 0; % propagation loss [micron^-1]; constant
L1_nomod=47.47+230.742;
L1_mod = 3000;
L2_nomod=90.605+3000+619.277; % Units [μm, microns], variable

% beta = spatial_frequency + j*loss
beta = @(neff_coeffs, lambda) ...
    (2*pi*neff_eq(neff_coeffs, lambda)./lambda - 1i*alpha/2*ones(1,length(lambda)) );

% beta w/ modulation voltage dependence neff = neff(0V) + dneff/dV * V
beta_push = @(neff_coeffs, V, lambda) ...
    (2*pi*(neff_eq(neff_coeffs, lambda)+sp*V)./lambda - 1i*alpha/2*ones(1,length(lambda)) );
beta_pull = @(neff_coeffs, V, lambda) ...
    (2*pi*(neff_eq(neff_coeffs, lambda)-sp*V)./lambda - 1i*alpha/2*ones(1,length(lambda)) );

% MZI transfer function with modulation on one arm (beta is dependent on
% voltage for one arm)
T_MZI = @(neff_coeffs, V, lambda) ...
    ( 0.25* abs(exp(-1i*(beta_push(neff_coeffs, V, lambda)*L1_mod+beta(neff_coeffs, lambda)*L1_nomod)) ...
    + exp(-1i*beta(neff_coeffs, lambda)*L2_nomod)).^2);

% Acquire MZI transfer function with different modulation voltages
lambda_min = 1.5; % Units [μm, microns]
lambda_max = 1.6;
lambda_step = 0.01e-3; % wavelength step [microns]
% Typical minimum step for a tunable laser is 1-10 pm.
lambda=linspace(lambda_min,lambda_max,lambda_step);
transmission_results = zeros(length(voltages), length(lambda));
for i = 1:length(voltages)
    transmission_results(i, :) = T_MZI(polymer.X, voltages(i), lambda);
end

%% Plot transmission vs. wavelength varying modulation voltage
figure(9)
hold on
for i = 1:length(voltages)
    plot(lambda, transmission_results(i, :), 'DisplayName', sprintf("V=%d", voltages(i)));
end
xlabel ('Wavelength [\mu m]');
ylabel ('Transmission');
axis tight
title ('MZI Transfer Function w/ varying modulation voltage');

```

```

legend
grid on

%% Simulate push-pull configuration
L2_mod = 3000;
L2_nomod=90.605+619.277; % Units [ $\mu\text{m}$ , microns], variable
T_MZI_pushpull = @(neff_coeffs, V, lambda) ...
    ( 0.25* abs(exp(-1i*(beta_push(neff_coeffs, V, lambda)*L1_mod+beta(neff_coeffs, lambda)*L1_nomod)) ...
        + exp(-1i*(beta_pull(neff_coeffs, V, lambda)*L2_mod+beta(neff_coeffs, lambda)*L2_nomod))).^2);
transmission_results_pushpull = zeros(length(voltages), length(lambdas))
for i = 1:length(voltages)
    transmission_results_pushpull(i, :) = T_MZI_pushpull(polymer.X, voltages(i), lambdas)
end

figure(10)
hold on
for i = 1:length(voltages)
    plot(lambdas, transmission_results_pushpull(i, :), 'DisplayName', sprintf("V=%d", voltages(i)));
end
xlabel ('Wavelength [ $\mu\text{m}$ ']);
ylabel ('Transmission');
axis tight
title ('MZI Transfer Function w/ varying modulation voltage, push-pull configuration');
legend
grid on

```

D. MATLAB code for fitting second order Taylor series model to n_{eff} vs. wavelength data from Lumerical MODE simulations

```

% User provides a matrix of neff values vs. wavelength from Lumerical
% Matlab curve fits 2nd order Taylor series about centre wavelength,
% lambda_o, and returns n1, n2, n3
%  $n_{\text{eff}}(\lambda) = n_1 + n_2(\lambda - \lambda_o) + n_3(\lambda - \lambda_o)^2$ 

%% Load Lumerical Results
% Mainly collecting effective index and frequency from results of frequency
% sweep in Lumerical. W = 500  $\mu\text{m}$ , t = 220 nm, SiO2-Si-Cladding
load("../LumericalResults\12042023\air_cladding_wg.mat");

%% Calculate 2nd order Taylor fit coefficients n1, n2, n3

% take the real part of the effective index.
neff = real(neff)

% speed of light, m/s
c=299792458;

% f is the matrix of frequency points,
% where the effective index is recorded.
lambdas = c ./ f;
lambdas = lambdas * 1e6 % convert to microns.
lambda0 = 1.55; % replace with desired centre wavelength

figure(1); plot (lambdas, neff, 'o', 'MarkerSize',10); hold on;

% use Matlab anonymous function for the effective index expression:
neff_eq = @(nx, lambda) (nx(1) + nx(2).*(lambda-lambda0) + nx(3).*(lambda-lambda0).^2);
X=[2.4 0 0]; % initial guess.
plot ( lambdas, neff_eq(X, lambdas), 'r' ) % Straight, horizontal line
format long

% curve fit to find expression for neff
X = lsqcurvefit (neff_eq, X, lambdas, neff);
disp("N_eff vs wavelength coefficients n1, n2, n3:")
disp(X)
r=corrcoef(neff,neff_eq(X, lambdas));
r2=r(1,2).^2;
disp ([ 'Goodness of fit, r^2 value: ' num2str(r2) ])

% Plot data
lambdas2=linspace(min(lambdas), max(lambdas), 100);

```

```

plot ( lambdas2, neff_eq(X, lambdas2), 'k')
xlabel ('Wavelength [um]');
ylabel ('Effective Index');
legend ('Data', 'Initial Guess', 'Curve Fit')

%% Plot effective index vs. wavelength for air and polymer cladding together
% Load 2nd order polynomial coefficients of the two waveguides
air = load("data\n_eff_vs_wavelength_coeffs_air_cladding.mat");
polymer = load("data\n_eff_vs_wavelength_coeffs_polymer_cladding.mat");

figure(2);
plot(lambdas2, neff_eq(air.X, lambdas2), "r", "LineWidth", 2);
hold on;
plot(lambdas2, neff_eq(polymer.X, lambdas2), "b", "LineWidth", 2)
xlabel('Wavelength [um]')
ylabel('Effective Index')
legend('Air cladding', 'HLD1/HLD2 cladding')
title('Effective index vs. wavelength')

% Include taylor series equation for fun
t = text(1.52, neff_eq(air.X, 1.52)+0.012, ...
    sprintf("%f + %f(\lambda-1.55) + %f(\lambda-1.55)^2", air.X(1), air.X(2), air.X(3)))
set(t, 'Rotation', -18);
t2 = text(1.52, neff_eq(polymer.X, 1.52)+0.012, ...
    sprintf("%f + %f(\lambda-1.55) + %f(\lambda-1.55)^2", polymer.X(1), polymer.X(2), polymer.X(3)))
set(t2, 'Rotation', -14);
grid on;

%% Extract group index from frequency sweep

air = load("../LumericalResults\12042023\air_cladding_wg.mat")
polymer = load("../LumericalResults\12042023\polymer_cladding_wg.mat")
c=299792458 % speed of light
air_ng = c./air.vg
polymer_ng = c./polymer.vg

%% Perform fit for group index too

% Select group index to curve fit
ng = polymer_ng

% speed of light, m/s
c=299792458;

% f is the matrix of frequency points,
% where the effective index is recorded.
lambdas = c ./ f;
lambdas = lambdas * 1e6 % convert to microns.
lambda0 = 1.55; % replace with desired centre wavelength

figure(3); plot (lambdas, ng,'o','MarkerSize',10); hold on;

% use Matlab anonymous function for the effective index expression:
ng_eq = @(nx, lambda) (nx(1) + nx(2).*(lambda-lambda0) + nx(3).*(lambda-lambda0).^2);
X=[2.4 0 0]; % initial guess.
plot ( lambdas, ng_eq(X, lambdas), 'r') % Straight, horizontal line
format long

% curve fit to find expression for neff
X = lsqcurvefit (ng_eq, X, lambdas, ng);
disp("N_g vs wavelength coefficients n1, n2, n3:")
disp(X)
r=corrcoef(ng,ng_eq(X, lambdas));
r2=r(1,2).^2;
disp ([ 'Goodness of fit, r^2 value: ' num2str(r2) ])

% Plot data
lambdas2=linspace(min(lambdas), max(lambdas), 100);
plot ( lambdas2, ng_eq(X, lambdas2), 'k')
xlabel ('Wavelength [um]');
ylabel ('Group Index');
legend ('Data', 'Initial Guess', 'Curve Fit')

```

```

%% Plot group index vs. wavelength for air and polymer cladding together
% Load 2nd order polynomial coefficients of the two waveguides
air = load("data\n_g_vs_wavelength_coeffs_air_cladding.mat");
polymer = load("data\n_g_vs_wavelength_coeffs_polymer_cladding.mat");

figure(3);
plot(lambdas2, ng_eq(air.X, lambdas2), "r", "LineWidth", 2);
hold on;
plot(lambdas2, ng_eq(polymer.X, lambdas2), "b", 'LineWidth', 2)
xlabel('Wavelength [\mu m]')
ylabel('Group Index')
legend('Air cladding', 'HLD1/HLD2 cladding')
title('Group index vs. wavelength')
grid on;

```

E. MATLAB code for fitting of MZI transfer function onto experimental data

```

%% Load data
V0 = load("active_data\12062023\0.mat")
name = "m0"

%% Plot calibration loopback
lambda=V0.wavelength
amplitude=V0.power(:, 1)
figure(1);
plot (lambda*1e6, amplitude);
title ('Calibration loopback');
xlabel ('Wavelength [\mu m]')
ylabel ('Insertion Loss [dBm]')
hold all;

%% Fit calibration loopback in wavelength of interest
% Fit the data with a polynomial
p=polyfit((lambda-mean(lambda))*1e6, amplitude, 5);
amplitude_LOOPBACK=polyval(p,(lambda-mean(lambda))*1e6);
plot (lambda*1e6, amplitude_LOOPBACK);
% find wavelength range with usable data, in the loopback
loopback_IL = max(amplitude);
new_lambda_i=find(amplitude>loopback_IL-10);
lambda=lambda(new_lambda_i);
lambda_min = min(lambda);
lambda_max = max(lambda);
amplitude=amplitude(new_lambda_i);
% refit the loopback
LOOPBACK=polyfit((lambda-mean(lambda))*1e6, amplitude, 4);
amplitude_LOOPBACK=polyval(LOOPBACK,(lambda-mean(lambda))*1e6);
plot (lambda*1e6, [amplitude_LOOPBACK], 'r-', 'Linewidth',5);
axis tight;
%% Find peak
center_lambda = find(amplitude_LOOPBACK == max(amplitude_LOOPBACK))
xline(lambda(center_lambda)*1e6)
%%

%% MZI data:
lambda1=V0.wavelength
amplitude=V0.power(:, 2)
figure(2);
plot (lambda1*1e6, amplitude);
title ('MZI (raw data)');
xlabel ('Wavelength [\mu m]')
ylabel ('Insertion Loss [dBm]')

%%

%%%%%%%%%%%%%
% MZI data - calibrated
%
% data only within the bandwidth of interest.
lambda=lambda_min:min(diff(lambda1)):lambda_max;
amplitude=interp1(lambda1, amplitude, lambda, 'linear');
amplitude(find(amplitude==inf))=-50;
% calibrate data
amplitude_cal=amplitude-polyval(LOOPBACK,(lambda-mean(lambda))*1e6);

```

```

figure(3);
plot (lambda, amplitude_cal);
hold on;
title ('MZI (calibrated with loopback)');
xlabel ('Wavelength [nm]')
ylabel ('Insertion Loss [dB]')

%%
amplitude = amplitude_cal
dL = 431.67; % [micron] Path length difference in the MZI
%%%%%%%%%%%%%
%%%%%%%%%%%%%
% Find ng from autocorrelation-based frequency estimation of spectrum
% auto-correction
[r,lags]=xcorr(amplitude);
r=r(ge(lags,0));
lags=lags(ge(lags,0));
figure(4)
plot(lags,r);
% estimate the frequency
d=diff(r);
start = find(gt(d,0)); start=start(1);
[peak_m, peak_i]=max(r(start:end));
peak_i=peak_i+start; % location of the 1st peak in the autocorrelation
hold on;
plot(peak_i,0,'s','MarkerSize',20);
title ('Autocorrelation of spectrum')
xlabel('lag, sample number');

fsr = peak_i * mean(diff(lambda))
ng_av = mean(lambda)^2/(dL*1e-6)/fsr
%%

% find starting point for curve fitting, using the ng value
% lambda0 is in microns.
lambda0 = mean(lambda) * 1e6;
n1=2.4;
%modeNumber = n1_initial * dL / lambda0 - 0.5;
%n1 = (2*floor(modeNumber)+1)*lambda0/2/dL;
n2 = (n1-ng_av)/lambda0;
nx_init = [n1 n2 0];
alpha_init = 1e-3; % propagation loss [micron^-1]
x0=[nx_init, alpha_init, -10]; % Initial guess: n1, n2, n3, alpha, excess loss

% Define the MZI transfer function
% - as a Taylor expansion around the central wavelength
% - Use units of [microns] - keeps the variables closer to 1.
% - These make the curve fitting easier.
% use Matlab anonymous functions
% effective index:
neff = @(nx, lambda) ...
    (nx(1) + nx(2).*(lambda-lambda0) + nx(3).*(lambda-lambda0).^2);
% neff([2.4, -1, 0], 1.56) % test it.
% alpha = 1e-3; % propagation loss [micron^-1]
% complex propagation constant
beta = @(nx, alpha, lambda) ...
    (2*pi*neff(nx, lambda)./lambda - 1i*alpha/2*ones(1,length(lambda)) );
% beta([2.4, -1, 0], 1e-3, [1.56, 1.57]) % test it.
% MZI transfer function
T_MZI = @(X, lambda) ...
    (10*log10( 0.25* abs(1+exp(-1i*beta(X(1:3), X(4), lambda)*dL)).^2 ) +X(5) );
% T_MZI([2.4, -1, 0, 1e-3], [1.56, 1.57]) % test it.

figure(5);
plot (lambda*1e6, amplitude);
hold all;
plot (lambda0, -40,'s','MarkerSize',20);
plot(lambda*1e6, T_MZI(x0, lambda*1e6),'--','LineWidth',3);
xlabel ('Wavelength [\mu m]');
ylabel ('Transmission [dB]');

```

```

axis tight
title ('MZI model (initial parameters)');
%%

% Autocorrelation again, to find the shift between the fit function and experimental data
[r,lags]=xcorr(amplitude, T_MZI(x0, lambda*1e6));
r=r(ge(lags,0));
lags=lags(ge(lags,0));
[peak_m, peak_i]=max(r);
lambda_offset = peak_i(1) * mean(diff(lambda));
n_shift = lambda_offset*lambda0/fsr/dL;
x0(1)=x0(1)+n_shift;

figure(6);
plot (lambda*1e6, amplitude);
hold all;
plot (lambda0, -40, 's', 'MarkerSize',20);
plot(lambda*1e6, T_MZI(x0, lambda*1e6), '--', 'LineWidth',3);
xlabel ('Wavelength [\mu m]');
ylabel ('Transmission [dB]');
axis tight
title ('MZI model (initial parameters, with shift)');

% Curve fit:
[xfit,resnorm] = lsqcurvefit(T_MZI,x0,lambda*1e6,amplitude);
xfit
r=corrcoef(amplitude,T_MZI(xfit, lambda*1e6));
r2=r(1,2).^2

figure(7);
plot (lambda*1e6, amplitude);
hold all;
plot(lambda*1e6, T_MZI(xfit, lambda*1e6), 'LineWidth',3);
xlabel ('Wavelength [\mu m]');
ylabel ('Transmission [dBm]');
axis tight
title ('MZI model fit for HLD1:HLD2 EO polymer clad MZM');
legend(["Experimental", "Model"])

% Check if the fit is good. If so, find ng
% plot ng curve
figure(8);
neff_fit = neff(xfit(1:3),lambda*1e6);
dndlambd=diff(neff_fit)./dnlambda; dndlambd=[dndlambd, dndlambd(end)];
ng=(neff_fit - lambda .* dndlambd);
plot(lambda*1e6, ng, 'LineWidth',4);
xlabel ('Wavelength [\mu m]');
ylabel ('Group index, n_g');
axis tight
title ('Group index from MZI fit for HLD1:HLD2 EO polymer clad MZM');

% waveguide parameters at lambda0
ng0 = xfit(1) - lambda0*xfit(2)

%% Compare simulation vs. experimental compact models
figure(9);
polymer_group_coeffs = load("data\n_g_vs_wavelength_coeffs_polymer_cladding.mat");
plot(lambda*1e6, ng, 'LineWidth',2)
hold on;
lambda0 = 1.55 % Switch central wavelength since that was what was used in simulation
plot(lambda*1e6, neff(polymer_group_coeffs.X, lambda*1e6), 'LineWidth', 2)
title('Group index vs. wavelength, HLD1:HLD2 Polymer Cladding')
xlabel('Wavelength [\mu m]')
ylabel('Group index')
legend('Experimental', 'Simulated')
grid on

```

F. MATLAB code for finding peaks from experimental data and calculating average FSR

```

%% Load data
V0 = load("active_data\12062023\0.mat")
name = "m0"

%% Plot calibration loopback
lambda=V0.wavelength
amplitude=V0.power(:, 1)
figure(1);
plot (lambda*1e6, amplitude);
title ('Calibration loopback');
xlabel ('Wavelength [\mu m]')
ylabel ('Insertion Loss [dBm]')
hold all;

%% Fit calibration loopback in wavelength of interest
% Fit the data with a polynomial
p=polyfit((lambda-mean(lambda))*1e6, amplitude, 5);
amplitude_LOOPBACK=polyval(p,(lambda-mean(lambda))*1e6);
plot (lambda*1e6, amplitude_LOOPBACK);
% find wavelength range with usable data, in the loopback
loopback_IL = max(amplitude);
new_lambda_i=find(amplitude>loopback_IL-10);
lambda=lambda(new_lambda_i);
lambda_min = min(lambda);
lambda_max = max(lambda);
amplitude=amplitude(new_lambda_i);
% refit the loopback
LOOPBACK=polyfit((lambda-mean(lambda))*1e6, amplitude, 4);
amplitude_LOOPBACK=polyval(LOOPBACK,(lambda-mean(lambda))*1e6);
plot (lambda*1e6, [amplitude_LOOPBACK],'r-','Linewidth',5);
axis tight;
%% Find peak
center_lambda = find(amplitude_LOOPBACK == max(amplitude_LOOPBACK))
xline(lambda(center_lambda)*1e6)
%%

% MZI data:
lambda1=V0.wavelength
amplitude=V0.power(:, 2)
figure(2);
plot (lambda1*1e6, amplitude);
title ('MZI (raw data)');
xlabel ('Wavelength [\mu m]')
ylabel ('Insertion Loss [dBm]')

%%

%%%%%%%%%%%%%
% MZI data - calibrated
%
% data only within the bandwidth of interest.
lambda=lambda_min:min(diff(lambda1)):lambda_max;
amplitude=interp1(lambda1, amplitude, lambda, 'linear');
amplitude(find(amplitude== -inf))=-50;
% calibrate data
amplitude_cal=amplitude-polyval(LOOPBACK,(lambda-mean(lambda))*1e6);
figure(3);
plot (lambda, amplitude_cal);
hold on;
title ('MZI (calibrated with loopback)');
xlabel ('Wavelength []')
ylabel ('Insertion Loss [dB]')

%% Smooth data
amplitude_cal_smooth = smoothdata(amplitude_cal, 'gaussian', 50)
plot(lambda*1e6, amplitude_cal_smooth);
legend(["No smoothing", "Smoothing"])

%% Find peaks
findpeaks(amplitude_cal_smooth,lambda);
[pks, locs] = findpeaks(amplitude_cal_smooth,lambda);

```

```
%% Calculate average FSR
npks = length(pk)
for n = 1:npks-1
    fsr(n) = locs(n+1) - locs(n)
end
average_fsr = mean(fsr)

%% Save to file
save(sprintf("peaks\\%s.mat", name), "average_fsr", "amplitude_cal_smooth", "lambda", "pk", "locs")
```